THE JOURNAL OF PHYSICAL CHEMISTRY A

Article

Cite This: J. Phys. Chem. A 2019, 123, 10109−10115

pubs.acs.org/JPCA

Infrared Spectroscopy of Hydrogen-Bonding Interactions in Neutral Dimethylamine−Methanol Complexes

Shukang Jiang,[†,‡,§,∥,○] Xiangtao Kong,[‡,○] Chong Wang,[‡,∥,○] Xiangyu Zang,[‡,∥] Mingzhi Su,[‡,∥] Huijun Zheng,[‡,∥] Bingbing Zhang,[‡] Gang Li,[‡] Hua Xie,[‡] Xueming Yang,[†,‡,§] Zhiling Liu,*[,⊥] Zhifeng Liu,*[,#,▽] and Ling Jiang*[,‡]

[†]Shanghai Advanced Research Institute, Chinese Academy of Sciences, 99 Haike Road, Zhangjiang Hi-Tech Park, Pudong, Shanghai 201210, China

[‡]State Key Laboratory of Molecular Reaction Dynamics, Dalian Institute of Chemical Physics, Chinese Academy of Sciences, 457 Zhongshan Road, Dalian 116023, China

[§]School of Physical Science and Technology, ShanghaiTech University, 393 Middle Huaxia Road, Pudong, Shanghai 201210, China

[∥]University of Chinese Academy of Sciences, 19A Yuquan Road, Beijing 100049, China

[⊥]School of Chemical and Material Science, Key Laboratory of Magnetic Molecules & Magnetic Information Materials, Ministry of Education, Shanxi Normal University, No. 1, Gongyuan Street, Linfen 041004, Shanxi, China

[#]Department of Chemistry and Centre for Scientific Modeling and Computation, Chinese University of Hong Kong, Shatin 999077, Hong Kong, China

[▽]CUHK Shenzhen Research Institute, No.10, 2nd Yuexing Road, Nanshan District, Shenzhen 518172, China

Supporting Information

ABSTRACT: Infrared spectra of the neutral dimethylamine−methanol cluster, DMA−CH_3OH, were measured in the spectral range of 2800−3900 cm^{-1} using an infrared-vacuum ultraviolet (IR-VUV) scheme. Quantum chemical calculations and ab initio molecular dynamic (AIMD) simulations were carried out to understand the experimental spectral features. Experimental and theoretical results reveal the coexistence of N···HO and O···HN hydrogen-bonded structures. AIMD simulations show that the methyl group in methanol internally rotates around the N···O axis, addressing the dynamic effect of the fluctuation of hydrogen bonds on the vibrational features. The bonding analysis was performed to elucidate the nature of the intermolecular interaction between DMA and CH_3OH. The present work provides the fundamental understanding of hydrogen-bonding networks in the amine−alcohol complexes.

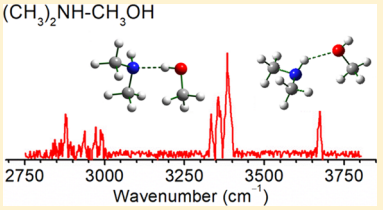

1. INTRODUCTION

Hydrogen bonds play an important role in chemistry, biology, and material science.[1] For instance, the hydrogen-bonding interactions have been recognized as one of the key factors in the nucleation and growth of atmospheric nanoparticles.[2] The presence of methylamines (monomethylamine (MMA), dimethylamine (DMA), and trimethylamine (TMA)) has been found ubiquitous in the atmosphere.[3] With hydrogen atoms substituted by methyl groups, methylamines have stronger basicity than ammonia and are expected to form more stable complexes with water and alcohols, which would enhance the interactions between amines and clusters/nanoparticles and aerosol nucleation.[3−5] In the fast-flow nucleation experiments involving sulfuric acid, water, and nitrogen-containing species (such as ammonia, DMA, and TMA), DMA was reported to enhance the nucleation process of sulfuric acid and water by a factor of ∼3.5.[6]

Studies on the hydrogen-bonding network in gaseous clusters have provided important knowledge on the structures and the dynamics that are difficult to extract from measurements in condense phases.[7−15] Microwave spectroscopy of the neutral TMA−water complex revealed the formation of a strong HOH···$N(CH_3)_3$ hydrogen bond in which the water molecule internally rotates around the symmetry axis of TMA.[16] Theoretical studies on the interaction between methylamine and water indicated that water molecules act as the donor for the formation of OH···N hydrogen bonds.[17,18] A closed ring with four hydrogen-bonded H_2O molecules was observed in the neutral $(TMA)_2(H_2O)_4$ clusters.[19] Infrared photodissociation (IRPD) spectra of protonated TMA−water clusters, $TMA−H^+−(H_2O)_n$ (n = 1−22), were measured in the OH stretching vibrational region,[20] which were different from those of $H^+(H_2O)_n$ and $(H_2O)_n$. In the $TMA−H^+−(H_2O)_n$ clusters, the proton (H^+) is always localized on the TMA moiety and would not be transferred to the water moiety even when the number of water molecules is large ($n \sim 20$).[20] The

Received: September 10, 2019
Revised: October 24, 2019
Published: October 29, 2019

DOI: 10.1021/acs.jpca.9b08630
J. Phys. Chem. A 2019, 123, 10109−10115

hydrogen-bonding networks of TMA−H^+−$(H_2O)_n$ (n = 1−3) are under the strong influence of the excess proton. These studies have provided great insights into the hydrogen-bonding structures and the dynamics of the TMA−water complexes.

DMA is a molecule with one polar NH group and two nonpolar CH_3 groups. The methanol molecule, CH_3OH, has one polar OH group and one nonpolar CH_3 group. The DMA−CH_3OH cluster therefore provides a model system for studying the hydrogen-bonding networks in the binary amine−alcohol complexes. A broad feature was observed at 3387 cm^{-1} in the IR spectra of the DMA−CH_3OH complex measured in a 10 cm cell, which was assigned to the hydrogen-bonded OH stretch of the N···HO structure.[21] Herein, we report the well-resolved IR spectra of the size-selected DMA−CH_3OH cluster in the spectral range of 2800−3900 cm^{-1}, which identify the coexistence of N···HO and O···HN hydrogen-bonded structures in the present experimental conditions. The experimental spectra are interpreted with the aid of quantum chemical calculations and ab initio molecular dynamic (AIMD) simulations. Chemical-bonding analysis was carried out to understand the nature of the intermolecular interaction between DMA and CH_3OH.

2. EXPERIMENTAL METHOD

IR spectra of the neutral dimethylamine−methanol complex were recorded using the Dalian IR-VUV spectrometer described previously.[22] A brief description is given here. The 118 nm VUV light was generated by third-harmonic generation (355 nm) of an Nd:YAG laser (Nimma-600) via a Xe/Ar gas mixture. Neutral complexes generated from supersonic expansions of a 3% DMA + 2% methanol/He mixture were ionized by the 118 nm VUV light in the center of the extraction region of a reflectron time-of-flight (TOF) mass spectrometer. Here, the tunable IR light pulse was introduced at about 50 ns prior to the VUV laser pulse in a crossed manner. The repetition frequencies of IR and 118 nm VUV laser were 10 and 20 Hz, respectively. IR spectrum of size-selected neutral cluster was recorded as a depletion spectrum of the monitored ion signal intensity by scanning the IR wavelength using the difference mode of operation (laser on−laser off), which was converted from the measured relative depletion of the mass spectrometric ion signal $(I(\nu)/I_0)$ upon IR irradiation to relative absorption cross sections $\sigma(\nu)$ using $\sigma(\nu) = -\ln[I(\nu)/I_0]/P(\nu)$. IR power dependence of the signal was measured to ensure that the predissociation yield is linear with the photon flux.

The IR laser pulse was produced by a LaserVision optical parametric oscillator/amplifier system (OPO/OPA).[23] This seeded table-top IR laser system generates 7 ns pulse with a spectral bandwidth of 1 cm^{-1}. The IR wavelength was calibrated using a wavelength meter (Bristol, 821 pulsed laser wavelength meter).

3. COMPUTATIONAL METHODS

Initial structures for optimization have been obtained from AIMD simulations, as implemented in the CP2K package,[24] which sampled the various conformations. The methods for the AIMD simulations have been described previously.[22] The BLYP functional with dispersion corrected by Grimme's D3 scheme was used.[25] The wave functions of double-zeta Gaussians were utilized. Only two types of structures were obtained from the AIMD simulations. The first type of structure consists of an N···HO hydrogen bond (labeled isomer I), and the second type of structure has an O···HN hydrogen bond (labeled isomer II), which is consistent with the previous studies.[21]

Quantum chemical calculations were performed using the Gaussian 09 package.[26] The structural optimization of isomers I and II was carried out using the MP2 method with the aug-cc-pVDZ basis set. Relative energies and energy barriers were calculated for 0 K structures, which include the zero-point vibrational corrections. The harmonic vibrational frequencies were scaled by a factor of 0.958, determined by the ratio of the experimental value (3681 cm^{-1})[27] to the MP2/aug-cc-pVDZ-calculated one (3841 cm^{-1}) of the OH stretch in the free CH_3OH molecule, which is consistent with the scaling factor reported previously.[28] The resulting stick spectra were convoluted by a Gaussian line shape function with an 8 cm^{-1} full width at half maximum (FWHM).

The dynamic motion of the clusters was computed by the AIMD approach. The vibrational spectrum was obtained by the Fourier transform of the dipole time-correlation function (DTCF).[22,29] Dynamic and anharmonic effects were automatically taken into accounts in such a scheme, although quantum effects at low temperature were not included.

Chemical bonding analyses were carried out by quantum theory of atoms in molecules (QTAIM),[30] noncovalent interactions (NCI),[31] and energy decomposition analysis with natural orbitals of chemical valence (EDA-NOCV).[32] The wave function files generated from MP2 calculations were utilized to analyze the topology of the electron density and NCI using the Multiwfn package.[33] The EDA-NOCV bonding was analyzed at the BP86-D3(BJ)/TZ2P level with the geometries optimized at the MP2/aug-cc-pVDZ level.

4. RESULTS AND DISCUSSION

4.1. Experimental Results. The $(DMA−CH_3OH)^+$ cation is obtained by the 118 nm single-photon ionization, and the number densities of the larger $[(DMA)_m(CH_3OH)_n]^+$ clusters are negligible (Figure S1). The $(DMA)_n^+$, $H^+(DMA)_m$, and H^+(DMA−CH_3OH) cations are observed as well. With a proton affinity ∼930 kJ/mol,[34] DMA could easily pick up a proton, which is similar to the VUV ionization of MMA, DMA, and TMA systems reported previously.[22,35,36] IR spectra of the neutral DMA−CH_3OH complex were recorded by monitoring the depletion for the intensity of the $(DMA−CH_3OH)^+$ mass channel. Figure 1a shows the experimental IR spectrum of neutral DMA−CH_3OH. The band positions are summarized in Table 1.

The experimental IR spectrum comprises five groups of bands labeled A−E in Figure 1a. Band A appears at 3674 cm^{-1}, which is 7 cm^{-1} red shifted from the OH stretch of the free CH_3OH molecule (3681 cm^{-1}).[27] Bands B−D appear at 3334−3384 cm^{-1}, which are in the spectral region of the free NH stretch and hydrogen-bonded OH/NH stretch.[22,35−38] The feature E (2843−2987 cm^{-1}) is in the CH stretching vibrational region.[22,35−38]

4.2. Harmonic IR Spectra. To understand the spectral features and the hydrogen-bonding structures of the neutral DMA−CH_3OH cluster, quantum chemical calculations were carried out to identify the structure of the low-lying isomers using the MP2/aug-cc-pVDZ method. The optimized structures of isomers I and II for the neutral DMA−CH_3OH cluster and their calculated harmonic IR spectra are illustrated in Figure 1b,c, respectively.

DOI: 10.1021/acs.jpca.9b08630
J. Phys. Chem. A 2019, 123, 10109−10115

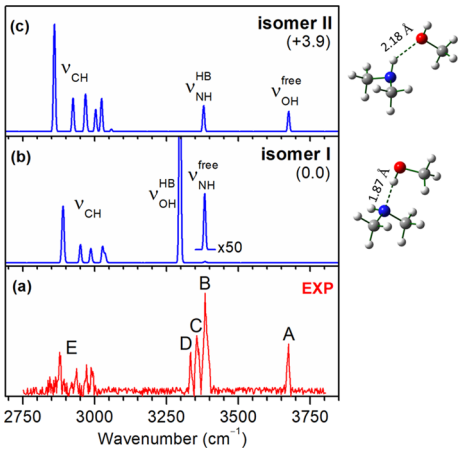

Figure 1. (a) Experimental IR spectrum of DMA−CH_3OH, with the MP2-calculated scaled harmonic IR spectra, structures, and relative energies (kcal/mol) of the two lowest-energy isomers (b) I and (c) II.

Table 1. Experimental and Calculated Band Positions (in cm^{-1}) and Assignments for Neutral DMA−CH_3OH Complex

label	expt	isomer I	isomer II	assignment
A	3674		3675	free OH stretch (ν_{OH}^{free})
B	3384	3383		free NH stretch (ν_{NH}^{free})
C	3356		3379	hydrogen-bonded NH stretch (ν_{NH}^{HB})
D	3334	3297		hydrogen-bonded OH stretch (ν_{OH}^{HB})
E	2987	3028	3024	CH stretch (ν_{CH})
	2971	2987	3004	
	2937	2951	2968	
	2877	2890	2925	
	2843		2860	

As shown in Figure 1, the lowest-energy isomer (isomer I) is held together by an N···HO hydrogen bond in which the hydrogen atom of the OH group acts as a donor for the hydrogen bond. Isomer II lies 3.9 kcal/mol higher in energy than isomer I and consists of an O···HN hydrogen bond in which the oxygen atom of the OH group acts as an acceptor for the hydrogen bond. The HB distance in isomer I is 1.87 Å, considerably shorter than the HB distance at 2.18 Å in isomer II, which indicates a more favorable hydrogen bond interaction in isomer I.

In the calculated IR spectrum of isomer I (Figure 1b), the free NH stretch (labeled ν_{NH}^{free}) is calculated at 3383 cm^{-1}, which is in agreement with the experimental value of band B (3384 cm^{-1}). The hydrogen-bonded OH stretch (labeled ν_{OH}^{HB}) is predicted at 3297 cm^{-1}, which is about 37 cm^{-1} lower than the experimental band D (3334 cm^{-1}). The calculated CH stretches (labeled ν_{CH}, 2890−3028 cm^{-1}) agree with the experimental feature E (2843−2987 cm^{-1}). The relative intensity of the free NH band was calculated to be very weak, while it appears very strong in the experimental spectrum (band B). Due to an internal vibrational redistribution (IVR) of the energy by IR photon absorption, the dissociation efficiency upon the IR-excited free NH vibrational mode is much larger than that upon the hydrogen-bonded NH vibrational mode.[39−41] Then, the experimental intensity of the free NH band is stronger than that of the hydrogen-bonded NH band, which has been manifested in the IRPD spectra of various hydrogen-bonded clusters.[13,14,20]

In the calculated IR spectrum of isomer II (Figure 1c), the free OH stretch (labeled ν_{OH}^{free}) is calculated at 3675 cm^{-1}, which is consistent with the experimental value of band A (3674 cm^{-1}). The hydrogen-bonded NH stretch (labeled ν_{NH}^{HB}) is predicted at 3379 cm^{-1}, which is in accord with the experimental band C (3356 cm^{-1}). The calculated CH stretches are in the 2860−3024 cm^{-1} region, which also match to the part of the experimental spectrum.

Summarizing, the calculated harmonic IR spectrum of isomer I qualitatively reproduces the experimental bands B, D, and E and that of isomer II agrees with the experimental bands A, C, and E. Accordingly, band A could be ascribed to the free OH stretch of isomer II (Table 1). Band B is assigned to the free NH stretch of isomer I. Band C is assigned to the hydrogen-bonded NH stretch of isomer II. Band D is due to the hydrogen-bonded OH stretch of isomer I. The CH stretches of isomers I and II are mainly responsible for band E. The difference between the experimental and calculated harmonic IR spectra in the 2850−3100 cm^{-1} region might be ascribed to the coupling between the CH stretching fundamental and bending overtone in a CH_3 group that was not considered in the harmonic calculations. Analogous CH stretch−bend Fermi couplings have been observed in the CH stretch region for a variety of hydrocarbon systems.[22,35,36,38,42−45] Recently, ab initio anharmonic vibrational calculations have been carried out to address the vibrational coupling of CH and NH stretches in the MMA and DMA clusters.[35,38] One cannot rule out the possibility for the presence of another Fermi Resonance peak. If band D is such a peak, then band B would be a hydrogen-bonded OH stretch and band C would be a hydrogen-bonded NH stretch. Examining such possibilities would require more sophisticated calculations that address not only IR frequencies and intensities but also higher-order vibrational excitations.

It thus appears that both isomers I and II contribute to the experimental spectrum. The isomerization barrier from isomer II to isomer I is calculated to be 9.1 kcal/mol at the MP2/aug-cc-pVDZ level, suggesting that this barrier could be sufficiently large such that supersonic expansion helium cooling is capable of kinetically trapping isomer II prior to its rearrangement to isomer I. Experimental observation of higher energy isomers on the potential energy surface has been reported in several cluster systems.[46−50] IR-VUV spectroscopic studies identified multiple coexisting structures have also been found for neutral ammonia and methylamine clusters,[22,35,36,51] suggesting that it is quite prevalent and could be detected by the IR-VUV scheme.

4.3. Ab Initio Molecular Dynamics Simulations. To address the dynamic nature of the weakly bonded DMA−CH_3OH complex and capture the vibrational features caused by the fluctuation in the distance of the hydrogen bond, AIMD simulations at finite temperatures were performed for the isomers I and II. The internal rotation of the methyl group unit in methanol (labeled $CH_3^{methanol}$) along the hydrogen bond was observed during the AIMD simulations (vide infra). The structural fluctuation is sensitive to the simulation temperature. At 40 K, isomer II is converted to isomer I, and above 50 K, the breaking of the hydrogen bond in the DMA−CH_3OH complex is observed. Representatively, the fluctuations in the N−H, O−H, C···C, C···N, and N···HO distances during AIMD simulations of isomer I at 30 and 40 K are illustrated in Figure 2. The DTCF spectra shown in Figure 3 were obtained by a data collection run in a duration of 50 ps. The trajectory

DOI: 10.1021/acs.jpca.9b08630
J. Phys. Chem. A 2019, 123, 10109−10115

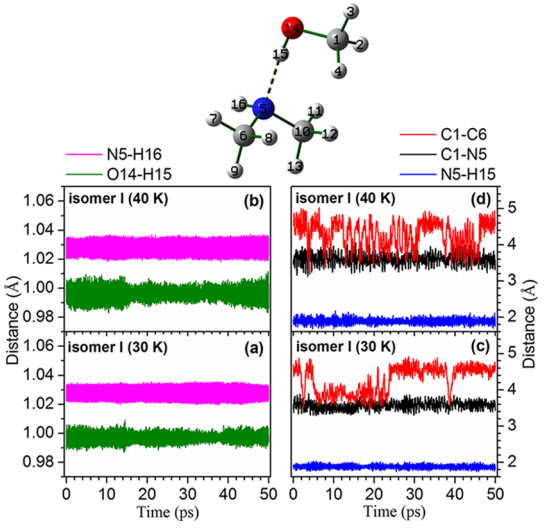

Figure 2. Fluctuation in the N−H, O−H, C···C, C···N, and N···HO distances during AIMD simulations of isomer I at 30 and 40 K.

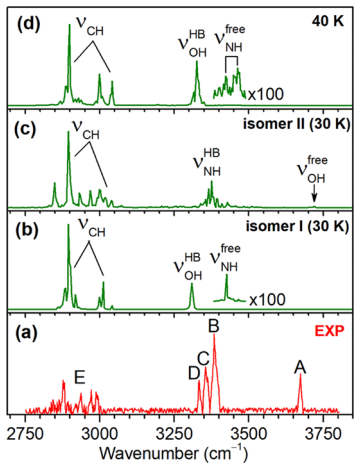

Figure 3. Comparison of the experimental IR spectrum (bottom) of neutral DMA−CH_3OH to dipole time-correlation function (DTCF) spectra from the AIMD simulations of isomers I and II at 30 and 40 K.

was first cut to 10 short pieces of 5 ps, each producing a spectrum, and these 10 spectra were then added together.

Our AIMD simulations show that the $CH_3^{methanol}$ group internally rotates around the hydrogen bond. Similarly, microwave spectroscopy of the TMA−water complex revealed a free rotation of the water molecule around the symmetry axis of TMA.[16] At a temperature of 30 K, the O14−H15 and N5−H16 bonds in isomer I fluctuate at 0.99−1.01 and 1.02−1.04 Å (Figure 2a), respectively; the intermolecular C1···N5 and N5···H15 distances fluctuate at 3.4−3.8 and 1.8−2.0 Å (Figure 2c), respectively, indicating that the hydrogen bond is maintained during the rotation of $CH_3^{methanol}$; the C1···C6 distance shows a larger amplitude fluctuation between 3.5 and 4.8 Å (Figure 2c), supporting the rotation feature of $CH_3^{methanol}$. When the temperature was raised to 40 K, the fluctuation amplitudes of N5−H16, O14−H15, C1···N5, and N5···H15 distances slightly increase as compared to those at 30 K (Figure 2b,d), whereas the C1···C6 distance fluctuates more frequently, revealing a faster rotation of $CH_3^{methanol}$.

In the DTCF spectra obtained from the AIMD simulation of isomer I at 30 K (Figure 3b), the ν_{NH}^{free} and ν_{OH}^{HB} peaks are at 3424 and 3309 cm^{-1}, respectively, which are closer to the experimental values of bands C and D. In the DTCF spectra of isomer I at 40 K (Figure 3c), the splitting of the ν_{NH}^{free} mode is observed at 3422 and 3458 cm^{-1}, which nicely reproduces the experimental bands C and B (3356 and 3384 cm^{-1}), respectively. Even though the $CH_3^{methanol}$ group unit rotates along the N···O axis in the DMA−CH_3OH cluster, the CH_3 group of methanol makes little contribution to the hydrogen-bonded NH and OH stretching region (Figure S2). On the other hand, the CH_3 group units of DMA also make negligible contribution to the hydrogen-bonded NH and OH stretching region. In the AIMD simulation at 40 K (Figure S2), there are some coupling between NH and OH stretching that produces the splitting.

With the hydrogen atom of water substituted by the methyl group, methanol would be expected to form a weaker N···HO hydrogen bond with methylamine than water. As reported previously, microwave spectroscopic studies indicated that the N···H distance in TMA−CH_3OH (1.92 Å) is longer than that in TMA−H_2O (1.82 Å).[16,52] The barrier for the $CH_3^{methanol}$ internal rotation in the TMA−CH_3OH complex was estimated to be ∼0.5 kcal/mol.[52] Considering the steric effect of the methyl group in the methanol, the barrier of the $CH_3^{methanol}$ internal motion would be larger than that of the water rotation. Indeed, microwave spectroscopy of the DMA−H_2O and TMA−H_2O complexes evidenced for a large-amplitude torsional or hindered torsional motion of the water about the hydrogen bond.[16,53] Such strong dynamics is expected to have a significant effect on the vibrational spectra of the methylamine−water clusters. To clarify the effect of the nonpolar methyl group in methanol as compared to water when these molecules bind to methylamine, further IR

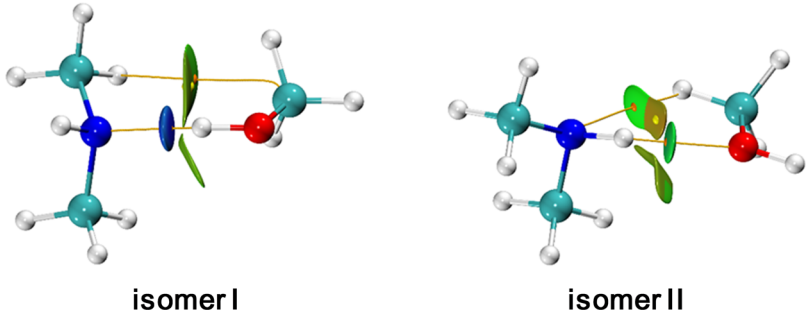

Figure 4. Color-filled NCI isosurfaces for isomers I and II of the DMA−CH_3OH complex: s = 0.5 and a blue-green-red color scale from −0.04 < sign(λ_2) $\rho(r)$ < +0.02 au. Small spheres represent critical points: BCPs in orange and RCPs in yellow.

DOI: 10.1021/acs.jpca.9b08630
J. Phys. Chem. A 2019, 123, 10109−10115

spectroscopic studies of the MA−water clusters (MA = MMA, DMA, TMA) are in progress and will be reported in a subsequent paper.

4.4. Bonding Analysis. To understand the nature of the intermolecular interaction between DMA and CH_3OH, both QTAIM and NCI indexes were computed from the electron density. As shown in Figure 4, the topology of isomers I and II is generally similar. For each isomer, there are clearly two bond critical points (BCPs; in orange) and the respective bond paths between the two fragments, which are accompanied by a ring critical point (RCP; in yellow) toward the center of the ring. The two BCPs in isomer I correspond to the intermolecular N···HO and C···HC interactions, while two BCPs in isomer II reveal the intermolecular O···HN and N···HC interactions. As depicted in Figure 4, the NCI isosurfaces highlight the complementarity of the NCI and AIM approaches. The nature of the intermolecular interactions in these two isomers is vividly illustrated in the scheme of continuous color coding. For isomer I, the blue and very disk-shaped isosurface in the intermolecular N···HO interaction region, which expands from BCP, corresponds to a typical strong hydrogen bond within the NCI framework. BCP in the C···HC interaction region is clearly marked by a distinct green isosurface, which corresponds to the weak intermolecular interaction and mixes with light-brown isosurface centered at RCP. The interaction region marked by the irregular flaky shaped isosurface could be identified as van der Waals interaction region, and its brown-green color shows that the electron density in this region is low. In contrast, both the two BCPs in isomer II are covered by the green isosurfaces, pointing to the weaker intermolecular interactions. This implies that the O···HN hydrogen bond interaction in isomer II is much weaker than the N···HO hydrogen bond interaction in isomer I, which is consistent with the calculated distances for the O···HN (2.18 Å) and N···HO (1.87 Å) hydrogen bonds (Figure 1).

The EDA-NOCV method has proven to give insight on the donor−acceptor interactions.[32] The numerical results obtained from the EDA-NOCV analyses for the isomers I and II are shown in Table 2. The intrinsic interaction energies ΔE_{int} between the frozen fragments indicate that isomer I has a stronger intermolecular interaction than isomer II, which is in accord with the calculated bond dissociation energies (D_e).

Table 2. EDA-NOCV Results of Isomers I and II for the DMA−CH_3OH Complex Calculated at the BP86-D3(BJ)/TZ2P Level[a]

parameter	isomer I	isomer II
ΔE_{int}	−9.02	−3.38
ΔE_{Pauli}	16.76	6.29
ΔE_{elstat}[b]	−14.43 (56.0%)	−5.32 (55.0%)
ΔE_{disp}[b]	−2.79 (10.8%)	−2.10 (21.7%)
ΔE_{orb}[b]	−8.56 (33.2%)	−2.25 (23.3%)
$\Delta E_{orb1(\sigma)}$[c]	−6.91 (80.7%)	−0.90 (40.0%)
$\Delta E_{orb(rest)}$[c]	−1.65 (19.3%)	−1.61 (60.0%)
ΔE_{prep}	0.29	0.15
$-D_e$	8.73	3.23

[a]The interacting fragments are DMA and CH_3OH in the electronic singlet states. Energy values are given in kilocalories per mole. [b]The values in parentheses give the percentage contribution to the total attractive interactions $\Delta E_{elstat} + \Delta E_{orb} + \Delta E_{disp.}$ [c]The values in parentheses give the percentage contribution to the total orbital interactions ΔE_{orb}.

Despite the larger contribution of the electrostatic interactions ΔE_{elstat} (55.0−56.0%) to stabilize the intermolecular interaction than that of the orbital interactions ΔE_{orb} (23.3−33.2%), ΔE_{elstat} is overcompensated by the Pauli repulsion energies (ΔE_{Pauli}) because of the repulsive interaction between the occupied lone-pair orbital of the N or O atom on one fragment and the occupied bonding orbital of the corresponding O−H or N−H bond on the other fragment. The dispersion interaction energies (ΔE_{disp}) provide the remaining 10.8−21.7% to the total attraction. It is clear from Table 2 that the ΔE_{orb} term in both isomers has one major component $\Delta E_{orb(\sigma)}$, with the remains coming from the intrafragment polarizations. Figure 5 shows the associated deformation densities $\Delta\rho$ for

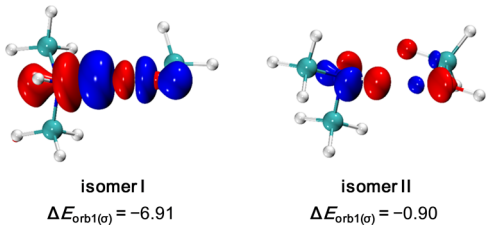

Figure 5. Plot of the deformation densities ($\Delta\rho$) of the pairwise orbital interactions between DMA and CH_3OH in the DMA−CH_3OH complex and associated stabilization energies ΔE (kcal/mol). The color code of the charge flow is red → blue.

isomers I and II, indicating the charge flow that is connected to the orbital interactions. The direction of the charge flow is indicated by the colors red → blue. Note that the $\Delta E_{orb1(\sigma)}$ component (−6.91 kcal/mol) in isomer I comes from the donation of the electron density from the lone pair of the nitrogen atom in DMA into the empty antibonding orbital of the O−H bond in CH_3OH. Such an orbital interaction weakens the O−H bond, which is manifested by the observed redshift of the hydrogen-bonded OH stretch in the experiment. In contrast, isomer II has a relatively weaker $\Delta E_{orb1(\sigma)}$ component (−0.90 kcal/mol) with respect to isomer I, which is mainly originated from the charge flow from the lone pair of the oxygen atom in the CH_3OH fragment into the empty antibonding orbital of the N−H bond in DMA. Thus, the QTAIM, NCI, and EDA-NOCV analysis results support the fact that the N···HO hydrogen bond interaction is stronger than the O···HN hydrogen bond interaction.[54]

5. CONCLUSIONS

The structures, energetics, and infrared spectra of the neutral DMA−CH_3OH cluster were studied using the IR-VUV spectroscopy combined with quantum chemical calculations, molecular dynamics simulation, and chemical bonding analyses. The results reveal the preferential formation of a strong N···HO hydrogen bond between DMA and CH_3OH in which the hydrogen atom of the OH group in CH_3OH acts as a donor for the hydrogen bond. The higher-energy structure with the O···HN hydrogen bond is also kinetically trapped in the present experiment. The vibrational features caused by the fluctuation in the distance of the hydrogen bond were addressed by the AIMD simulations. The present model should have important implications for hydrogen-bonding networks in the amine−alcohol complexes. It will be interesting to study the structures and dynamics of larger complexes.

DOI: 10.1021/acs.jpca.9b08630
J. Phys. Chem. A 2019, 123, 10109−10115

■ ASSOCIATED CONTENT

Supporting Information

The Supporting Information is available free of charge on the ACS Publications website at DOI: 10.1021/acs.jpca.9b08630.

Mass spectrum of the cluster cations (Figure S1) and DTCF spectra and DOS plots obtained from the AIMD simulations of isomer I at 30 and 40 K (Figure S2) (PDF)

■ AUTHOR INFORMATION

Corresponding Authors

*E-mail: lzling@sxnu.edu.cn (Z.L.).
*E-mail: zfliu@cuhk.edu.hk (Z.L.).
*E-mail: ljiang@dicp.ac.cn (L.J.).

ORCID

Hua Xie: 0000-0003-2091-6457
Xueming Yang: 0000-0001-6684-9187
Zhiling Liu: 0000-0002-1669-396X
Zhifeng Liu: 0000-0002-6898-075X
Ling Jiang: 0000-0002-8485-8893

Author Contributions

○S.J., X.K., and C.W. contributed equally to this work.

Notes

The authors declare no competing financial interest.

■ ACKNOWLEDGMENTS

This work was supported by the National Natural Science Foundation of China (grants 21473151, 21603130, 21673231, and 21688102), Dalian Institute of Chemical Physics (DICP DCLS201702), the Strategic Priority Research Program (Grant XDB17000000) of the Chinese Academy of Science, and the 1331 Engineering of Shanxi Province.

■ REFERENCES

(1) Hobza, P.; Havlas, Z. Blue-Shifting Hydrogen Bonds. *Chem. Rev.* **2000**, *100*, 4253−4264.
(2) Zhang, R.; Khalizov, A.; Wang, L.; Hu, M.; Xu, W. Nucleation and Growth of Nanoparticles in the Atmosphere. *Chem. Rev.* **2012**, *112*, 1957−2011.
(3) Qiu, C.; Zhang, R. Multiphase Chemistry of Atmospheric Amines. *Phys. Chem. Chem. Phys.* **2013**, *15*, 5738−5752.
(4) Yao, L.; et al. Atmospheric New Particle Formation from Sulfuric Acid and Amines in a Chinese Megacity. *Science* **2018**, *361*, 278−281.
(5) Kulmala, M.; et al. Direct Observations of Atmospheric Aerosol Nucleation. *Science* **2013**, *339*, 943−946.
(6) Yu, H.; McGraw, R.; Lee, S.-H. Effects of Amines on Formation of sub-3 nm Particles and Their Subsequent Growth. *Geophys. Res. Lett.* **2012**, *39*, L02807.
(7) Scherer, J. J.; Paul, J. B.; O'keefe, A.; Saykally, R. J. Cavity Ringdown Laser Absorption Spectroscopy: History, Development, and Application to Pulsed Molecular Beams. *Chem. Rev.* **1997**, *97*, 25−52.
(8) Buck, U.; Huisken, F. Infrared Spectroscopy of Size-Selected Water and Methanol Clusters. *Chem. Rev.* **2000**, *100*, 3863−3890.
(9) Robertson, W. H.; Johnson, M. A. Molecular Aspects of Halide Ion Hydration: The Cluster Approach. *Annu. Rev. Phys. Chem.* **2003**, *54*, 173−213.
(10) Wang, X.-B.; Wang, L.-S. Photoelectron Spectroscopy of Multiply Charged Anions. *Annu. Rev. Phys. Chem.* **2009**, *60*, 105−126.
(11) Rizzo, T. R.; Stearns, J. A.; Boyarkin, O. V. Spectroscopic Studies of Cold, Gas-Phase Biomolecular Ions. *Int. Rev. Phys. Chem.* **2009**, *28*, 481−515.
(12) Matsuda, Y.; Mikami, N.; Fujii, A. Vibrational Spectroscopy of Size-Selected Neutral and Cationic Clusters Combined with Vacuum-Ultraviolet One-Photon Ionization Detection. *Phys. Chem. Chem. Phys.* **2009**, *11*, 1279−1290.
(13) Fujii, A.; Mizuse, K. Infrared Spectroscopic Studies on Hydrogen-Bonded Water Networks in Gas Phase Clusters. *Int. Rev. Phys. Chem.* **2013**, *32*, 266−307.
(14) Heine, N.; Asmis, K. R. Cryogenic Ion Trap Vibrational Spectroscopy of Hydrogen-Bonded Clusters Relevant to Atmospheric Chemistry. *Int. Rev. Phys. Chem.* **2014**, *34*, 1−34.
(15) Dopfer, O.; Fujii, M. Probing Solvation Dynamics around Aromatic and Biological Molecules at the Single-Molecular Level. *Chem. Rev* **2016**, *116*, 5432−5463.
(16) Tubergen, M. J.; Kuczkowski, R. L. Microwave Spectroscopic Characterization of a Strong Hydrogen Bond: Trimethylamine-Water. *J. Am. Chem. Soc.* **1993**, *115*, 9263−9266.
(17) Sánchez-Lozano, M.; Cabaleiro-Lago, E. M.; Hermida-Ramón, J. M.; Estévez, C. M. A Computational Study of the Protonation of Simple Amines in Water Clusters. *Phys. Chem. Chem. Phys.* **2013**, *15*, 18204−18216.
(18) Mmereki, B. T.; Donaldson, D. J. Ab Initio and Density Functional Study of Complexes between the Methylamines and Water. *J. Phys. Chem. A* **2002**, *106*, 3185−3190.
(19) Rozenberg, M.; Loewenschuss, A.; Nielsen, C. J. H-Bonded Clusters in the Trimethylamine/Water System: A Matrix Isolation and Computational Study. *J. Phys. Chem. A* **2012**, *116*, 4089−4096.
(20) Shishido, R.; Li, Y.-C.; Tsai, C.-W.; Bing, D.; Fujii, A.; Kuo, J.-L. An Infrared Spectroscopic and Theoretical Study on $(CH_3)_3N$-H^+-$(H_2O)_n$, n = 1-22: Highly Polarized Hydrogen Bond Networks of Hydrated Clusters. *Phys. Chem. Chem. Phys.* **2015**, *17*, 25863−25876.
(21) Du, L.; Mackeprang, K.; Kjaergaard, H. G. Fundamental and Overtone Vibrational Spectroscopy, Enthalpy of Hydrogen Bond Formation and Equilibrium Constant Determination of the Methanol-Dimethylamine Complex. *Phys. Chem. Chem. Phys.* **2013**, *15*, 10194−10206.
(22) Zhang, B.; et al. Infrared-Vacuum Ultraviolet Spectroscopic and Theoretical Study of Neutral Methylamine Dimer. *J. Phys. Chem. A* **2017**, *121*, 7176−7182.
(23) Bosenberg, W. R.; Guyer, D. R. Broadly Tunable, Single-Frequency Optical Parametric Frequency-Conversion System. *J. Opt. Soc. Am. B* **1993**, *10*, 1716−1722.
(24) VandeVondele, J.; Krack, M.; Mohamed, F.; Parrinello, M.; Chassaing, T.; Hutter, J. QUICKSTEP: Fast and Accurate Density Functional Calculations Using A Mixed Gaussian and Plane Waves Approach. *Comput. Phys. Commun.* **2005**, *167*, 103−128.
(25) Grimme, S.; Antony, J.; Ehrlich, S.; Krieg, H. A Consistent and Accurate Ab Initio Parametrization of Density Functional Dispersion Correction (DFT-D) for The 94 Elements H-Pu. *J. Chem. Phys.* **2010**, *132*, 154104.
(26) Frisch, M. J. et al. *Gaussian 09, Revision E.01*; Gaussian, Inc.: Wallingford, CT, USA, 2013.
(27) Shimanouchi, T. *Tables of Molecular Vibrational Frequencies*; Vol. I ed.; Nat. Stand. Ref. Data Ser., 1972.
(28) Sinha, P.; Boesch, S. E.; Gu, C.; Wheeler, R. A.; Wilson, A. K. Harmonic Vibrational Frequencies: Scaling Factors for HF, B3LYP, and MP2 Methods in Combination with Correlation Consistent Basis Sets. *J. Phys. Chem. A* **2004**, *108*, 9213−9217.
(29) McQuarrie, D. A. *Statistic Mechanics*; Harper-Collins Publishers; New York. 1976.
(30) Bader, R. F. W. Atoms in Molecules. *Acc. Chem. Res.* **1985**, *18*, 9−15.
(31) Johnson, E. R.; Keinan, S.; Mori-Sánchez, P.; Contreras-García, J.; Cohen, A. J.; Yang, W. Revealing Noncovalent Interactions. *J. Am. Chem. Soc.* **2010**, *132*, 6498−6506.
(32) Mitoraj, M. P.; Michalak, A.; Ziegler, T. A Combined Charge and Energy Decomposition Scheme for Bond Analysis. *J. Chem. Theory Comput.* **2009**, *5*, 962−975.
(33) Lu, T.; Chen, F. Multiwfn: A Multifunctional Wavefunction Analyzer. *J. Comput. Chem.* **2012**, *33*, 580−592.

DOI: 10.1021/acs.jpca.9b08630
J. Phys. Chem. A 2019, 123, 10109−10115

(34) Hunter, E. P. L.; Lias, S. G. Evaluated Gas Phase Basicities and Proton Affinities of Molecules: An Update. *J. Phys. Chem. Ref. Data* **1998**, *27*, 413−656.
(35) Zhang, B.; et al. Infrared Spectra of Neutral Dimethylamine Clusters: An Infrared-Vacuum Ultraviolet Spectroscopic and Anharmonic Vibrational Calculation Study. *J. Chem. Phys.* **2019**, *150*, No. 064317.
(36) Zhang, B.-B.; Kong, X.-T.; Jiang, S.-K.; Zhao, Z.; Xie, H.; Hao, C.; Dai, D.-X.; Yang, X.-M.; Jiang, L. Infrared-Vacuum Ultraviolet Spectroscopic and Theoretical Study of Neutral Trimethylamine Dimer. *Chin. J. Chem. Phys.* **2017**, *30*, 691−695.
(37) Han, H.-L.; Camacho, C.; Witek, H. A.; Lee, Y.-P. Infrared Absorption of Methanol Clusters $(CH_3OH)_n$ with n = 2-6 Recorded with a Time-Of-Flight Mass Spectrometer Using Infrared Depletion and Vacuum-Ultraviolet Ionization. *J. Chem. Phys.* **2011**, *134*, 144309.
(38) Huang, Q.-R.; Li, Y.-C.; Ho, K.-L.; Kuo, J.-L. Vibrational Spectra of Small Methylamine Clusters Accessed by an Ab Initio Anharmonic Approach. *Phys. Chem. Chem. Phys.* **2018**, *20*, 7653−7660.
(39) Asmis, K. R.; Neumark, D. M. Vibrational Spectroscopy of Microhydrated Conjugate Base Anions. *Acc. Chem. Res.* **2012**, *45*, 43−52.
(40) King, D. S. Infrared Multiphoton Excitation and Dissociation. *Adv. Chem. Phys.* **1982**, *50*, 105−189.
(41) Mukamel, S.; Jortner, J. Multiphoton Molecular Dissociation in Intense Laser Fields. *J. Chem. Phys.* **1976**, *65*, 5204−5225.
(42) Tabor, D. P.; Kusaka, R.; Walsh, P. S.; Sibert, E. L., III; Zwier, T. S. Isomer-Specific Spectroscopy of Benzene-$(H_2O)_n$, n = 6,7: Benzene's Role in Reshaping Water's Three-Dimensional Networks. *J. Phys. Chem. Lett.* **2015**, *6*, 1989−1995.
(43) Sibert, E. L., III; Tabor, D. P.; Kidwell, N. M.; Dean, J. C.; Zwier, T. S. Fermi Resonance Effects in the Vibrational Spectroscopy of Methyl and Methoxy Groups. *J. Phys. Chem. A* **2014**, *118*, 11272−11281.
(44) Sibert, E. L., III; Kidwell, N. M.; Zwier, T. S. A First-Principles Model of Fermi Resonance in the Alkyl CH Stretch Region: Application to Hydronaphthalenes, Indanes, and Cyclohexane. *J. Phys. Chem. B* **2014**, *118*, 8236−8245.
(45) Buchanan, E. G.; Dean, J. C.; Zwier, T. S.; Sibert, E. L., III Towards a First-Principles Model of Fermi Resonance in the Alkyl CH Stretch Region: Application to 1,2-Diphenylethane and 2,2,2-Paracyclophane. *J. Chem. Phys.* **2013**, *138*, No. 064308.
(46) Douberly, G. E.; Miller, R. E.; Xantheas, S. S. Formation of Exotic Networks of Water Clusters in Helium Droplets Facilitated by the Presence of Neon Atoms. *J. Am. Chem. Soc.* **2017**, *139*, 4152−4156.
(47) Hou, G.-L.; Kong, X.-T.; Valiev, M.; Jiang, L.; Wang, X.-B. Probing the Early Stages of Solvation of cis-Pinate Dianions by Water, Acetonitrile, and Methanol: A Photoelectron Spectroscopy and Theoretical Study. *Phys. Chem. Chem. Phys.* **2016**, *18*, 3628−3637.
(48) Brites, V.; Cimas, A.; Spezia, R.; Sieffert, N.; Lisy, J. M.; Gaigeot, M.-P. Stalking Higher Energy Conformers on the Potential Energy Surface of Charged Species. *J. Chem. Theory Comput.* **2015**, *11*, 871−883.
(49) Yang, B.; Rodgers, M. T. Alkali Metal Cation Binding Affinities of Cytosine in the Gas Phase: Revisited. *Phys. Chem. Chem. Phys.* **2014**, *16*, 16110−16120.
(50) Goebbert, D. J.; Wende, T.; Jiang, L.; Meijer, G.; Sanov, A.; Asmis, K. R. IR Spectroscopic Characterization of the Thermally Induced Isomerization in Carbon Disulfide Dimer Anions. *J. Phys. Chem. Lett.* **2010**, *1*, 2465−2469.
(51) Matsuda, Y.; Mori, M.; Hachiya, M.; Fujii, A.; Mikami, N. Infrared spectroscopy of size-selected neutral clusters combined with vacuum-ultraviolet-photoionization mass spectrometry. *Chem. Phys. Lett.* **2006**, *422*, 378−381.
(52) Tan, X.-Q.; Ioannou, I. I.; Foltz, K. B.; Kuczkowski, R. L. The Methanol·Trimethylamine Complex: Structure and Large Amplitude Motions. *J. Mol. Spectrosc.* **1996**, *177*, 181−193.
(53) Tubergen, M. J.; Kuczkowski, R. L. Hydrogen Bonding to Dimethylamine: the Microwave Spectrum and Structure of the Dimethylamine-Water Complex. *J. Mol. Struct.* **1995**, *352-353*, 335−344.
(54) Hunter, C. A. Quantifying Intermolecular Interactions: Guidelines for the Molecular Recognition Toolbox. *Angew. Chem., Int. Ed.* **2004**, *43*, 5310−5324.

DOI: 10.1021/acs.jpca.9b08630
J. Phys. Chem. A 2019, 123, 10109−10115